Generation and applications of terahertz pulses with extreme high field

Final report

Principal investigator: Prof. Hebling, János

1. Development of high-energy THz sources

The development of highest-energy THz sources was the general aim of the project together with developing new applications for them. The main topics within THz source development were:

- investigation of pump pulse width and temperature effects on THz pulse generation,
- increasing the energy of THz pulses,
- development of the contact-grating technology.

a. Pump pulse width and temperature effects on THz pulse generation

In our paper published in 2011 (Fülöp et al., Opt. Express **19** (2011) 15090), with the help of model calculations, we pointed out that to achieve the largest possible THz energies it is advantageous to use longer, 500–600 fs pump pulses, rather than the commonly used 100 fs. In 2012 we experimentally confirmed that in case of 1.3 ps long pump pulses the efficiency of THz pulse generation increases significantly as compared to 100-fs pumping (Fülöp et al., Opt. Lett. **37** (2012) 557). The model calculations also indicated that cooling the $LiNbO_3$ crystal used in the THz source to cryogenic temperature can significantly increase the energy of THz pulses and their generation efficiency.

In 2013, in the frame of a Swiss-Hungarian-French collaboration, involving partners both from academia and industry, we carried out a series of measurements abroad, in which THz generation at room temperature was compared to that at 25 K, and the Fourier-limited pump pulse duration was set to four different values between 380 fs and 650 fs (Figure 1). The maximum pumping energy was 12 mJ. These detailed measurements showed that the THz pulse energy increases with increasing pump pulse length and decreasing temperature, in accordance with the model calculations. However, unlike the predictions from the model calculations, the THz energy was increasing further for pump pulses longer than 500 fs. The reason for the deviation between theory and prediction needs further investigation. The results summarized here were published in the paper Vicario et al., Opt. Lett. **38** (2013) 5373.

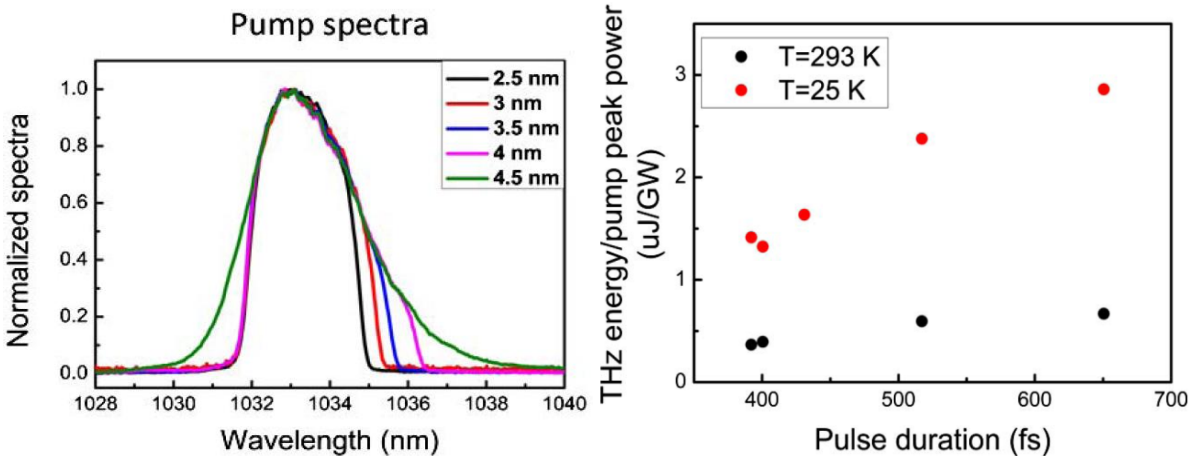

*Figure 1. Left: Pump pulse spectra for different spectral cuts. Right: THz pulse energy normalized to the pump peak power as function of the laser pulse duration at T=293 K and T=25 K. From Vicario et al., Opt. Lett. **38** (2013) 5373.*

b. Increasing the energy of THz pulses

In 2012 we performed the experiments in Garching, which resulted in the generation of THz pulses with the highest (125 μJ) energy at that time, obtained from optical rectification (Fülöp et al., Opt. Lett. **37** (2012) 557). These measurements clearly showed the potential of using longer pump pulses for high-energy THz pulse generation. However, the pump pulses used in these experiment were much too long, and in addition, they were not transform limited.

In 2013 we performed another series of measurements in Garching. At this time the pump pulse duration was shorter, about 780 fs, and nearly transform limited. Under such improved conditions we were able to achieve a new record in THz energy. THz pulses with more than 0.4 mJ energy were generated at room temperature by using an optimized imaging telescope for pulse-front tilt (Figure 2a). The pump-to-THz conversion efficiency was increased from the previous 0.25% to 0.77% (Figure 2b).

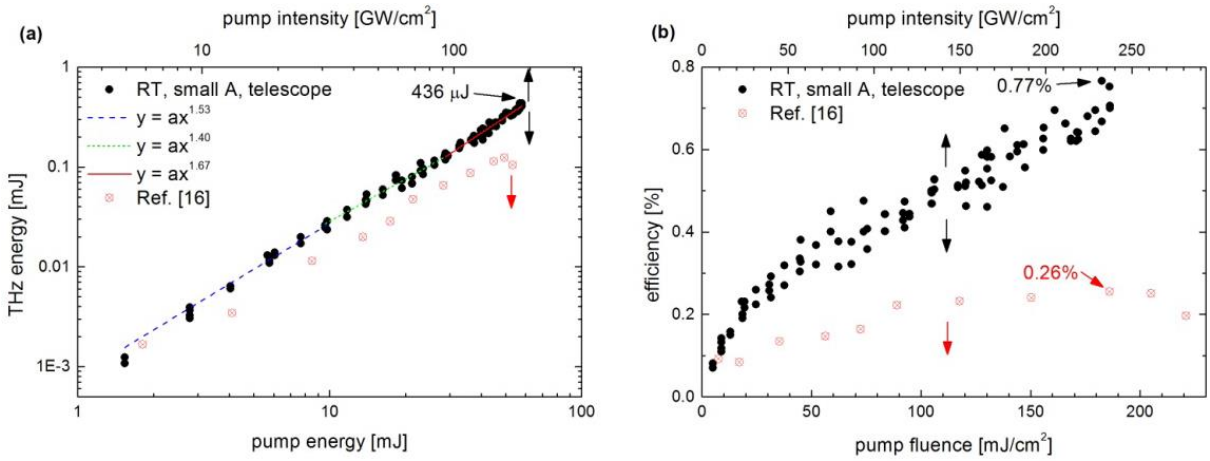

*Figure 2. Measured THz energy vs. pump energy and intensity (a), and the corresponding efficiencies vs. pump fluence and intensity (b). Empty red symbols are from our previous experiment (Fülöp et al., Opt. Lett. **37** (2012) 557). Both intensity scales refer only to the present experiment, as indicated by arrows. From Fülöp et al., Opt. Express **22** (2014) 20155.*

According to the predictions of our calculations and the results of our small-scale experiments (see above, Vicario et al., Opt. Lett. **38** (2013) 5373), another important contribution to increasing the THz generation efficiency is cooling the generating $LiNbO_3$ crystal to cryogenic temperatures. This reduces the absorption of the crystal at THz frequencies. We also carried out a comparative study at room temperature (RT) and at cryogenic temperature (CT) to verify the scalability of increased efficiency to high THz pulse energies. We measured 0.23% efficiency at RT, which could be increased to 0.62% at CT (Figure 3). In the latter case the THz energy was 186 μJ.

Taken together, we have experimentally demonstrated the generation of highest-energy THz pulses with high (close to 1%) conversion efficiency. This verifies the theoretically predicted scaling of the THz efficiency with pump pulse duration and crystal temperature, and the expectation that the 1-mJ THz energy barrier can be achieved with ~100 mJ pump pulse energy. The demonstrated THz pulse parameters enable their application to particle-acceleration. The results summarized here were published in the paper Fülöp et al., Opt. Express **22** (2014) 20155.

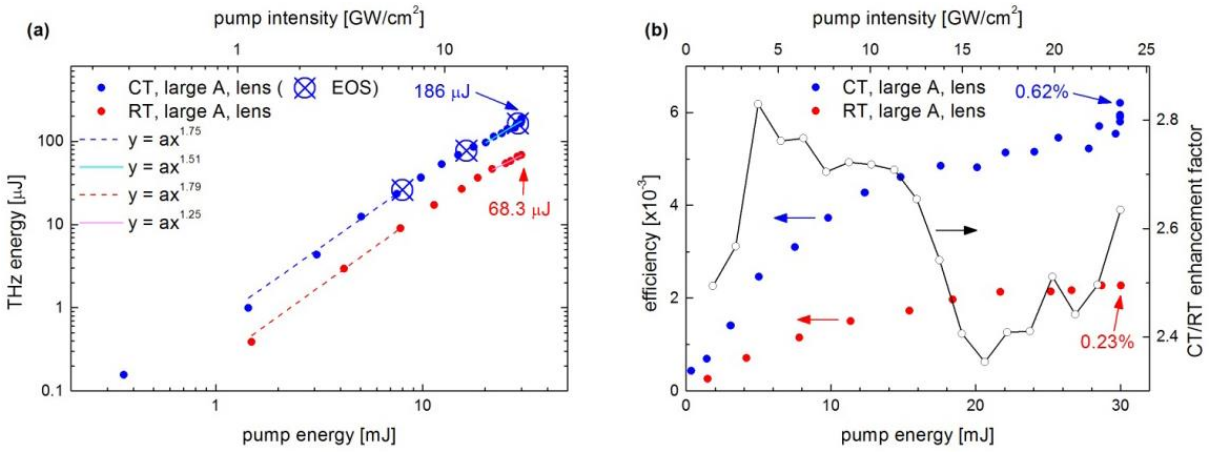

*Figure 3. (a) Measured THz energy vs. pump energy and intensity at RT and CT. The large crossed symbols refer to measurement points where electro-optic sampling was also carried out. (b) The corresponding conversion efficiencies vs. pump energy and intensity at CT and RT. The ratio of the CT and RT efficiencies, obtained by interpolation, is shown by the empty symbols. From Fülöp et al., Opt. Express **22** (2014) 20155.*

c. Development of the contact-grating technology

Significant increase in THz pulse energy and generation efficiency can be expected from the contact-grating technology, which we proposed in 2008. This is a compact realization of the tilted-pulse-front pumping scheme, where no imaging optics is used. Imaging optics can lead to distortions of the pump pulse front, thereby limiting the useful pump spot size and the useful pump energy.

We have analysed a possible practical realization of the contact-grating scheme based on $LiNbO_3$ in our paper in 2012 (Ollmann et al., Appl. Phys. B **108** (2012) 821). We have shown that diffraction efficiency as high as 99% can be achieved with a suitable design (Figure 4).

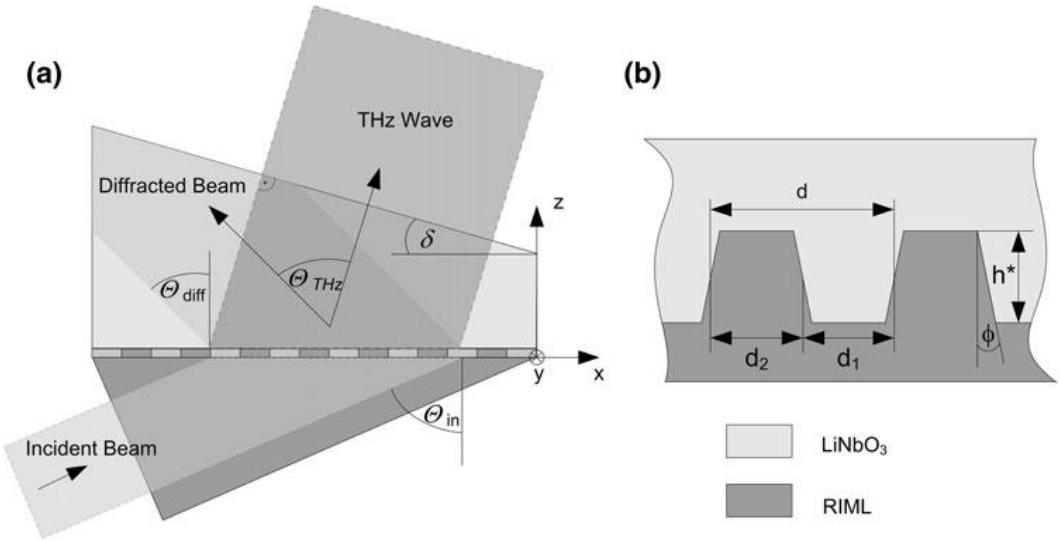

*Figure 4. (a) Side view of the contact-grating setup. (b) Grating profile. From Ollmann et al., Appl. Phys. B **108** (2012) 821.*

However, the technical realization turned out to be very challenging. The reason for this is the required high groove density (<400 nm period) and the large binary profile depth (~500 nm), which should cover at least 1 cm^2 area. Examples of realized grating profiles are shown in Figure 5. While the target profile was a binary one with 90° wall angle, the etched wall angle was only about 75°, which significantly reduces the diffraction efficiency, and consequently, the achievable pump-to-THz conversion efficiency.

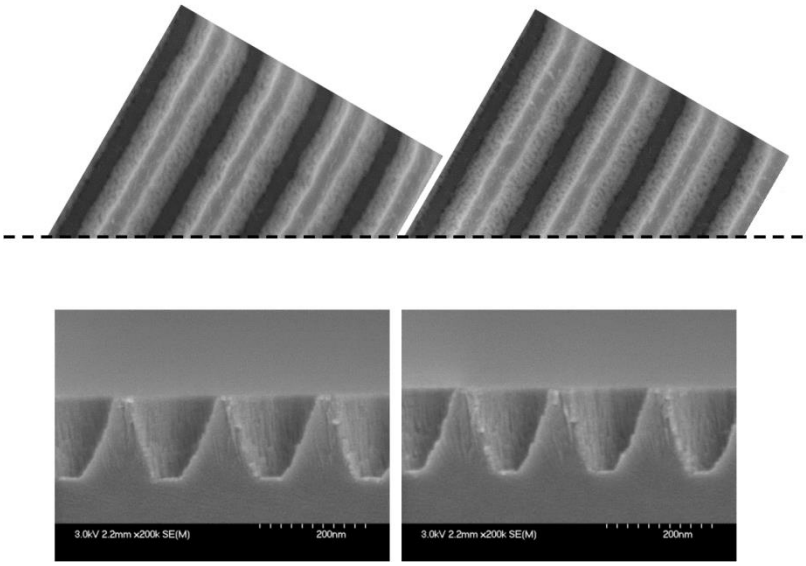

Figure 5. Scanning electron microscope images of cross-sections of grating profiles on $LiNbO_3$.

In order to overcome these technical challenges, we followed another approach. In our previous theoretical work from 2010 (Fülöp et al., Opt. Express **18** (2012) 12311) we predicted that semiconductors have high potential for realizing high-energy THz sources when pumped at longer (>1.5–1.8 µm) wavelengths using tilted-pulse-front pumping. The important advantage of semiconductor nonlinear materials for realizing a contact-grating THz source is the larger grating period (>1 µm), in combination with a shallower profile. This is due to the longer pump wavelength and the required small pulse-front-tilt angles, typically in the range of 10 to 30°. We carried out the detailed design for a ZnTe-based contact grating (Ollmann et al., Opt. Commun. **315** (2014) 159). It is also possible to design a grating where the incoming pump beam and the generated THz beam are collinear. Our calculations predict that it is possible to generate THz pulses with mJ energy from a ZnTe contact-grating source of a few cm size. Our industrial collaboration partners performed successful etch tests on ZnTe (Figure 6). We expect that prototype gratings will be soon at our disposal and THz generation experiments can be tackled in the near future.

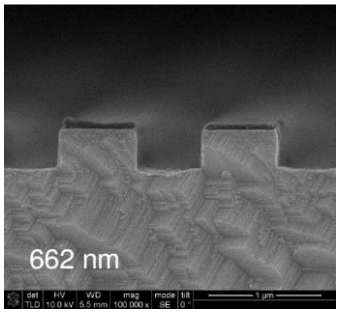

Figure 6. One example of good quality binary grating profile on ZnTe.

2. Applications of intense THz pulses

a. Acceleration of charged-particle beams

The most important, but also largest and most expensive research facilities are particle accelerators. Because of this, there is a strong effort to make these devices more compact and cost effective. Laser-based accelerators were proposed to achieve this goal. According to numerical studies, with dielectric laser accelerators (DLAs) based on a double-grating dielectric structure it is possible to achieve loaded gradients exceeding 1 GeV/m [1]. Very recently, the working of such a miniature accelerator was

demonstrated in proof-of-principle experiments [2]. However, these results also show the drawback of this approach: for a laser with about 1 µm wavelength the gap between the dielectric structures (see also Figure 7a) can only be a few hundred nm, thereby limiting the charge of the accelerated electron/ion bunch.

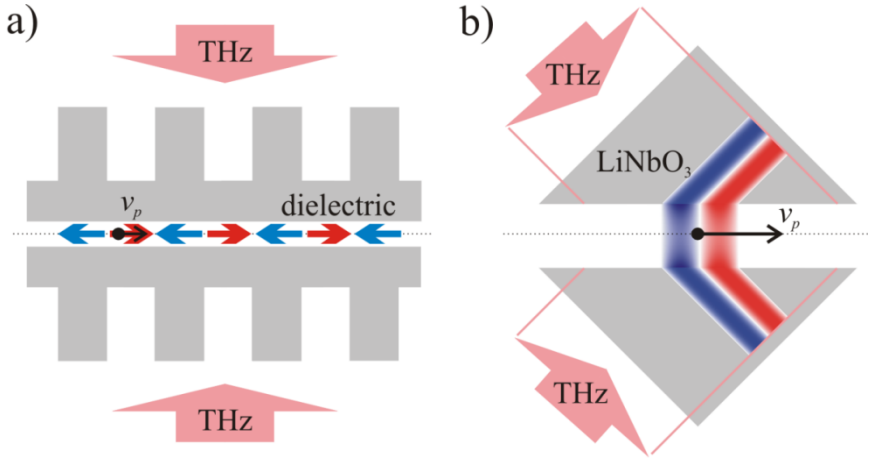

Figure 7. Scheme of the THz-driven electron (a) and proton (b) acceleration.

In a recent publication we drew the attention to the fact that THz pulses with extremely high field strength available at present or becoming available in the near future, owing to their two orders of magnitude longer wavelength, are better suited for charged particle manipulation, including acceleration, bending, and spatial or temporal focusing [3].

It was shown by numerical simulations that by using 20-mJ, 0.6-THz driving pulses for electron acceleration in dielectric-loaded metallic waveguides it is possible to accelerate a 1.6-pC electron bunch from 1 MeV to 10 MeV by simultaneously compressing it from 100 fs to 2 fs [4]. For such a device, and similarly for dielectric grating accelerators [1,2,5], using THz driving pulses rather than visible/near-infrared ones enables to exploit advantages of the two-to-three orders of magnitude longer wavelength and oscillation period of THz pulses. By using THz pulses larger transversal size allows larger bunch charge and results in larger throughput. Longer temporal period also allows a larger temporal jitter tolerance between the electron bunch and the driving pulse.

Nowadays with tilted-pulse-front-excitation [6] in $LiNbO_3$ (LN) THz energy on the mJ level and electric field strength of MV/cm can be reached (J. A. Fülöp et al., Opt. Express, **22** (2014) 20155). In the next few years using optimal conditions (contact grating, long-pulse excitation, and cryogenic temperatures) will expectedly result in THz pulses with 10 MV/cm focused electric field strength and energies on the tens-of-mJ level [7] enough for particle accelerator applications.

In 2014 we introduced (Z. Tibai et al., 4th EOS Topical Meeting on Terahertz Science & Technology, TST 2014) a dielectric THz-pulse-driven electron accelerator (DTA, Figure 7a). A setup for manipulation (post-acceleration and monochromatization) of protons/ions by intense THz pulses was also proposed in our paper (L. Pálfalvi et al., Phys. Rev. ST Accel. Beams **17** (2014) 031301), as shown in Figure 7b.

According to our simulations, post-acceleration of relativistic electrons can be realized by driving the above mentioned DTA setup (Figure 7a) with high-energy THz pulses. Based on calculation results, using dielectric grating length of 5 cm and nearly 20 mJ THz pulses with 0.33 and 0.7 THz frequencies, electrons with 1 MeV initial energy can be accelerated to 4 and 6.5 MeV, respectively.

Hadron therapy requires particle beams with ~100 MeV/nucleon energy and relative energy fluctuation on the order of 1%. Laser-driven accelerators produce ion beams with only tens of MeV/nucleon energy and extremely broad spectra.

In order to reach sufficient particle energy and sufficiently low energy fluctuation for hadron therapy we proposed a setup for post-acceleration and monochromatization of laser-generated protons by THz pulses (L. Pálfalvi et al., Phys. Rev. ST Accel. Beams **17** (2014) 031301). It is based on the idea of using the evanescent field of THz electromagnetic pulses between a pair of dielectric crystals as is shown in Figure 7b. An important advantage of the THz-driven accelerator is that the 0.1–0.5 THz frequency range naturally fits in wavelength to practical sizes of proton beams generated in laser-driven proton accelerators and hence enough spatial gap is ensured between the dielectric prisms allowing a large number of particles to pass through the structure. Moreover, contrary to laser fields, the approximately one-ps oscillation period of the THz pulses enables accurate timing between the accelerating THz field and the particle bunch. This is necessary for effective acceleration and monochromatization. The other advantage of the longer pulse duration is the increased acceleration length, without dephasing between the THz field and the particles.

For efficient acceleration and monochromatization the precise adjustment of the sweep velocity of the THz pulses to the velocity of the particles is needed. This can be achieved by the appropriate choice of the incidence angle of the THz beam at the vacuum-dielectric surface. The timing between the THz pulse and the incoming particles also have to be accurately adjusted. This can be achieve by using common (split) pump pulses to drive the laser proton accelerator and the THz source. In order to reach the necessary energy a few accelerator stages can be cascaded as described in our paper (L. Pálfalvi et al., Phys. Rev. ST Accel. Beams **17** (2014) 031301), thereby also allowing the precise adjustment of the synchronization during the acceleration process.

Since the value of damage threshold at the THz wavelength is unknown for LN in the model calculations modest value of about 1 MV/cm THz electric field strength was supposed. By simple model calculations we showed, that the energy of a proton bunch can be increased from 40 to 56 MeV in five stages and its initially broad energy distribution can be significantly reduced (below 1%).

The realization of the acceleration methods introduced above requires more detailed theoretical investigations and practical considerations. An important limiting factor is the damage of the dielectric materials caused by the intense THz pulses. Searching possible materials with high THz damage threshold are planned in the near future.

References to Section 2a

[1] T. Plettner et al., Phys. Rev. Spec. Top. Accel. Beams **9** (2006) 111301
[2] E. A. Peralta et al., Nature **503** (2013) 91-97
[3] J. Hebling et al., arXiv.org, arXiv:1109.6852 (2011)
[4] L. J. Wong et al, Optics Express **21** (2013) 9792-9806
[5] A. Aimidula et al., Nucl. Instr. Meth. A **19** (2014) 15090
[6] J. Hebling et al., Opt. Express **10** (2002) 1161
[7] J. A. Fülöp et al., Opt. Express **19** (2011) 15090

b. THz-driven strong-field electron emission from a gold surface

During the last few years, in the frame of this and other projects, we set up the first THz laboratory in Hungary, the High-Field THz Laboratory at University of Pécs. Presently, this laboratory provides 10-µJ level THz pulses and is continuously being developed further. One of our ongoing experiments

reported below aims at the study of THz-driven electron emission from a metal surface. This work is done in collaboration with the Wigner Institute in Budapest (Gy. Farkas, P. Dombi, I. Márton).

Photoemission of electrons from atoms or metal surfaces is a fundamental process in radiation-matter interaction and has been studied extensively using optical excitation. Electron emission driven by high-intensity light fields is accompanied by high-harmonic generation (HHG), a process forming the basis for attosecond technology. The photoelectric effect shows a characteristic nonlinear behaviour at moderate intensities, where $\gamma \gg 1$ holds for the Keldysh parameter. At very high intensities ($\gamma \ll 1$), (optical) field emission plays a dominant role. One unique feature of THz irradiation is the extremely low photon energy compared to the work function (about 5.2 eV for gold), and consequently, the extremely high order of nonlinearity $n{\sim}10^3$ for $\gamma \gg 1$. The other unique feature of THz radiation is that the transition from multiphoton to field emission region, characterized by $\gamma{\sim}1$, can be accessed by much smaller pulse energies (μJ) than in case of optical pulses, owing to the ${\sim}10^3$ times lower frequency.

In our experiment THz pulses are generated in $LiNbO_3$ by optical rectification of femtosecond laser pulses with tilted pulse front (Figure 8). Electro-optic sampling is used to measure the time dependence of the THz electric field. Single-cycle THz pulses with up to about 300 kV/cm peak electric field strength at 0.35 THz central frequency are illuminating the gold surface. An electron multiplier chain is used to amplify the photocurrent signal.

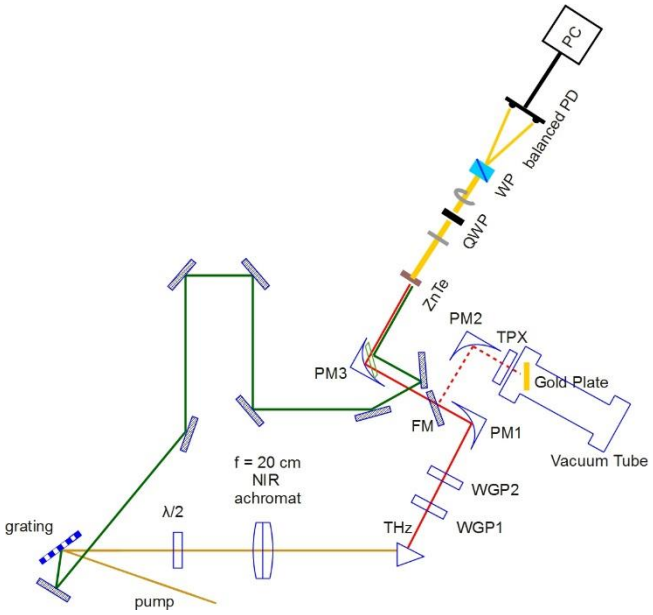

Figure 8. Experimental setup showing the THz source, the electro-optic sampling system for measuring the time-dependent electric field, and the electron multiplier tube with the illuminated gold surface.

Figure 9a shows the photocurrent measured at 45°angle of incidence, amplified by the electron multiplier (EM) at different bias voltages, as function of the THz electric field in this transition region. Significant electron emission was observed even at moderate field strengths. Interestingly, rotating the polarization of the THz beam resulted in triple maxima of the photocurrent (Figure 9b; $E_\perp$ is the field component perpendicular to the gold surface). The detailed description of the observed behaviour should include the interference of incident and reflected electric fields near the surface, possible effects of surface roughness, and the detector response. The results of this ongoing work will be presented at the OTST 2015 conference. We also plan to publish the results in a refereed journal paper.

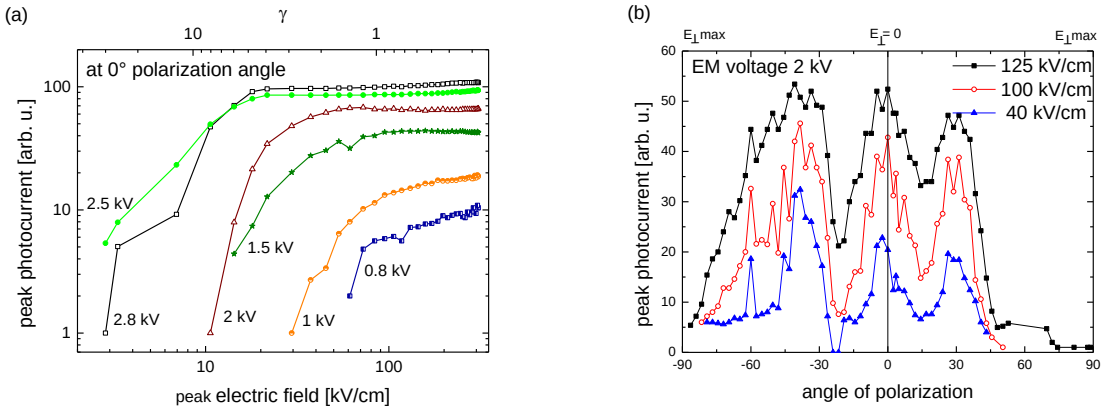

Figure 9. Measured photoemission signal vs. THz peak electric field for different electron multiplier (EM) bias voltages (left) and photocurrent vs. projected angle between the THz polarization direction and gold surface normal at 45° angle of incidence (right).

3. Proposal for EUV-VUV pulse generation with controlled carrier-envelope phase

The generation of waveform-controlled single- or few-cycle electromagnetic pulses down to the EUV or X-ray wavelengths is of considerable interest for a number of intriguing applications in spectroscopy of ultrafast processes [1]. EUV pump—EUV probe experiments can be carried out at free-electron lasers (FELs) [2-3]; however, the temporal resolution is limited to the fs regime. Various schemes, such as the longitudinal space charge amplifier [4], or two-color enhanced self-amplified spontaneous emission (SASE) [5] were proposed for attosecond pulse generation at FELs. A very recent scheme suggests possible generation of sub-attosecond pulses in the hard X-ray [6]. Although generation of carrier-envelope-phase (CEP) stabilized fs pulses in the VIS-NIR wavelength range is well established, currently there are no techniques available for CEP control of attosecond pulses in the EUV-VUV range, to the best of our knowledge. We proposed a robust method for producing waveform- and CEP- controlled few-cycle attosecond pulses in the EUV–VUV spectral range in 2014 (Z. Tibai et al., Phys. Rev. Lett. **113** (2014) 104801).

The proposed setup

Our proposed setup is shown in Figure 10. The method is based on coherent undulator radiation emitted by relativistic ultrathin electron layers, which are produced by nanobunching of a subpicosecond electron bunch, obtained from microwave electron accelerators (LINACs), in a double-period modulator undulator (MU) driven by a few-TW visible laser.

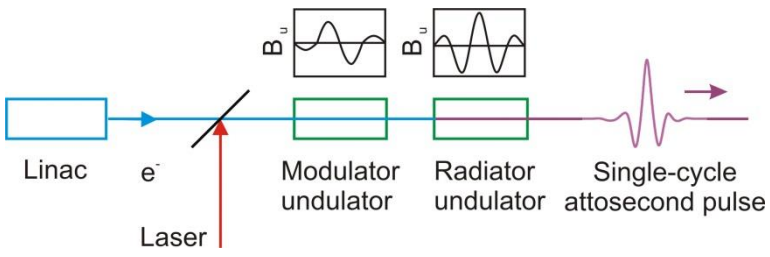

Figure 10. Scheme of the proposed setup.

Production of ultrathin electron layers by IFEL

According to our simulation the production of ultrathin electron layers is possible by nanobunching of ultrashort electron bunches by inverse free-electron laser (IFEL) interaction. We used the General Particle Tracer (GPT) [7] numerical code for the simulation of the nanobunching by the IFEL process. In the simulations, for the parameter of the electron bunch before the nanobunching we used the

bunch parameter of an existing injector [8-9], and the parameters are listed in Table 1. Calculated snapshots of distributions of macroparticles after nanobunching by the IFEL process are shown in Figure 11. **Hiba! A hivatkozási forrás nem található.** According to this the microbunch length is only 6 nm.

Table 1. Parameters used in most of the simulations.

Parameter	Value
E-beam energy (γ)	2000
E-beam intrinsic energy spread (1σ)	0.05 %
E-beam charge (total pulse)	≈ 0.25 nC
E-beam length (1σ)	≈ 30 µm
E-beam normalized emittance	1.4 mm mrad
E-beam radius	30 µm
Laser wavelength (λ_l)	0.516 µm
Laser power	10 TW
Laser beam waist inside MU	0.72 mm
MU period length (λ_{MU})	2.3 m
Undulator parameter of MU (K_{MU})	1.4

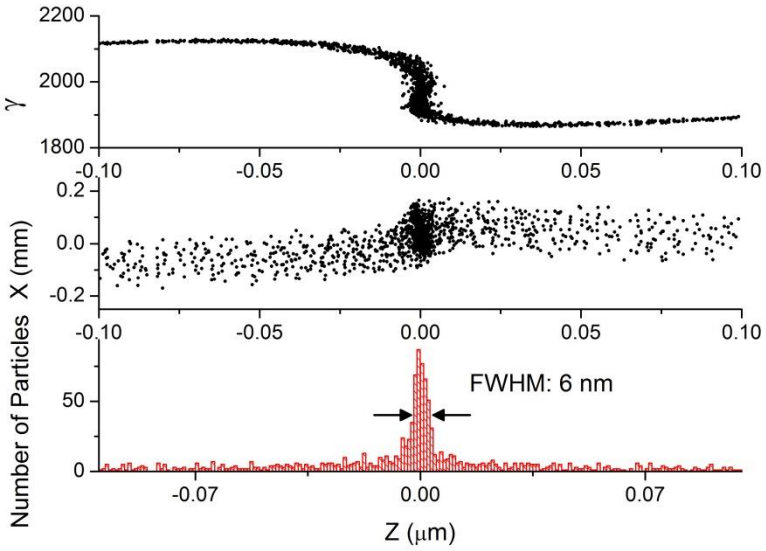

Figure 11. Snapshots of distributions of macroparticles after compression by the IFEL process. The panels show the relativistic factor γ, the spatial distribution in the x-z plane, and the distribution along the z axis.

Calculation method of electric field and results

We used the following handbook formula to calculate the temporal shape of the electric field of the radiation generated in a second undulator [10]:

(1)
$$\vec{E}(\vec{t},\vec{r}) = \left[\frac{q\mu_0}{4\pi}\frac{\vec{R}\times\left(\left(\vec{R}-R\vec{\beta}\right)\times\dot{\vec{\beta}}\right)}{\left(\vec{R}-R\vec{\beta}\right)^3}\right]_{ret}$$

where q is the electric charge of a macroparticle, μ_0 is the vacuum permeability, $\vec{R}$ is the vector pointing from the position of the charge at the retarded moment to the observation point, $\vec{v}$ is the

velocity of the macroparticle, and $\vec{\beta} = \vec{v}/c$, where c is the speed of light, and N is the number of the macroparticles.

During the radiation process the acceleration, velocity and position of the macroparticles were followed numerically by taking into account the Lorentz force equation:

(2) $$\frac{d(\gamma m\vec{v})}{dt} = q \cdot \vec{v} \times \vec{B}\big(z(t)\big),$$

where m is the mass of the charged particles, respectively, and $\vec{B}$ is the undulator magnetic field. The Coulomb interaction between the macroparticles was neglected during the undulator radiation process. This simplification is justified by the short interaction time. The electric field was calculated in a plane perpendicular to the propagation direction of the electron microbunch situated at 8 m behind the middle of the second undulator.

In a series of calculations electron bunches with a relativistic factor of γ = 2000 and an undulator with a few different magnetic field distributions were considered. Figure a displays the longitudinal distribution of the magnetic field for a five-dipole RU along the electron beam propagation direction, and the simulated waveform of the generated attosecond pulse. The generated CEP-controlled XUV waveforms with same spectra is shown in Figure b. The results of these calculations are indicating the versatility of our proposed method for generating ultrashort pulses.

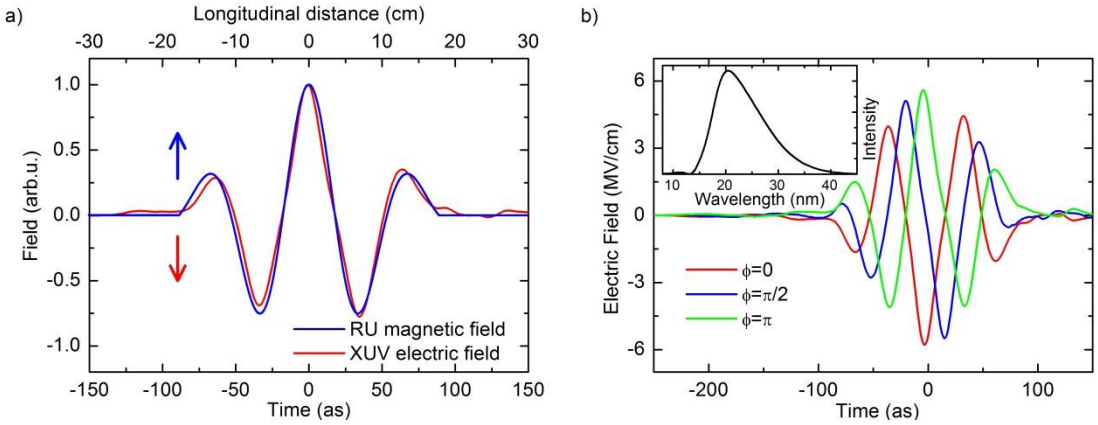

Figure 12. (a) Magnetic field distribution of RU (blue line) and the electric field of the generated attosecond pulse (red line). (b) CEP-controlled XUV waveforms with same spectra (inset). γ = 2000 in all cases.

In another series of calculations the relativistic factor was varied in the range of γ = 1000÷2000 and the λ_u undulator period was chosen such that for each value of γ the radiation wavelength was kept at a value of λ_r = 20 nm. According to the calculations the generation of single-cycle attosecond pulses with 23÷280 nJ energy is possible. Naturally, with this method attosecond pulses with linear or circular polarization can be generated in the VUV spectral range (10-200 nm). Depending on the generated wavelength, the energy of the pulses in case of circular polarization is 27÷285 nJ.

In another series of calculations the initial spatial distributions of the electrons was random, but the electron bunch length was kept constant for each run. There the CEP stability was investigated, and according to our calculations the standard deviations of the CEP are 31 and 13 mrad at 20 nm and 60 nm cases.

Conclusion and future plans

We proposed a robust method for producing few-cycle pulses with prescribed shaped in the EUV–VUV spectral range by coherent undulator radiation of relativistic ultrathin electron layers, which are

produced by IFEL. These attosecond pulse energies are high enough to use these pulses for example as pump pulses in pump-probe measurements. Pulses with the predicted exceptional parameters can enable time- and CEP-resolved measurements with sub-100-as resolution.

These results were published in the paper Tibai et al., Phys. Rev. Lett. 113 (2014) 104801, and were presented at 7 international conferences. The presentation at the SPIE conference in Prague was invited talk. The investigation of the feasibility of this method and the possibility of generation circularly polarized attosecond pulses are in progress and we plan to publish them in the near future.

4. Spatiotemporal focusing dynamics in plasmas at X-ray wavelength

Increasing laser peak power and intensity is one of the most important challenges for laser science and technology. Several schemes are proposed to achieve the short duration powerful X-ray pulses and focusing X-ray beams. However, these focusing techniques can withstand only low intensity X-ray pulse and might not be directly applicable to powerful LCLS X-ray pulse where focusing appears to be more challenging. Therefore, we proposed that by utilizing the backward Raman amplification (BRA) technique the X-ray laser pulse duration can be compressed to the electron plasma wave period [11]. We investigated the spatiotemporal focusing dynamics of a laser pulse in plasmas at X-ray wavelength. The simulation results demonstrate that spatiotemporal focusing dynamics in plasmas can be controlled with the appropriate choice of beam-plasma parameters to explore the high intensity effects in X-ray regime.

With our proposed setup (Z. Tibai et al., Phys. Rev. Lett. **113** (2014) 104801) described in Section 3, the intensity of the attosecond pulses is about 30 GW/cm^2 and the spot size 1 mm^2. Our recently proposed focusing technique may provide an opportunity to further decrease the spot size and increase the intensity.

References to Sections 3 and 4

[1] Reiter, et al., Phys. Rev. Lett. **105** (2010) 243902
[2] Y. Jiang et al., Phys. Rev. Lett. **105** (2010) 263002
[3] M. Magrakvelidze et al., Phys. Rev. A **86** (2012) 013415
[4] A. Marinelli et al., Phys. Rev. Lett. **110** (2013) 064804
[5] A. A. Zholents and G. Penn, Phys. Rev. ST Accel. Beams **8** (2005) 050704
[6] J. Dunning et al., Phys. Rev. Lett. **110** (2013) 104801
[7] www.pulsar.nl/gpt
[8] K. Honkavaara et. al., “Status of the FLASH II Project”, in Proceedings of the 34th International Free-Electron Laser Conference, (FEL2012, Nara, Japan, 2012), Report No. WEPD07
[9] S. Ackermann et al., “Optimization of HHG Seeding between 10 nm to 40 nm”, in Proceedings of the 34th International Free-Electron Laser Conference, (FEL2012, Nara, Japan, 2012), Report No. TUPD11
[10] J. D. Jackson: Classical Electrodynamics 3rd ed., Wiley, ISBN 0-471-30932-X
[11] A. Sharma et al., Phys. of Plasmas **21** (2014) 033103